Electrostatic Reconnection in the Ionosphere

J.D. Huba[1], T.-W. Wu[1], and J.J. Makela[2]
[1] Plasma Physics Division, Naval Research Laboratory, Washington, D.C., USA
[2] University of Illinois at Urbana-Champaign, Department of Electrical and and Computer Engineering, Urbana, IL, USA

ABSTRACT

Nighttime equatorial plasma bubble merging is examined using the NRL code SAMI3/ESF. It is found that bubbles merge through an 'electrostatic reconnection' process. As multiple bubbles develop, the electrostatic potential associated with one bubble can connect with that of a neighboring bubble: this provides a pathway for the low density plasma in one bubble to flow into the adjoining bubble and merge with it. Additionally high-speed plasma channels ($\gtrsim$ 100s m/s) can develop during the merging process. Optical data is presented of equatorial plasma bubble evolution that suggests bubble merging occurs in the nighttime equatorial ionosphere.

1. INTRODUCTION

The equatorial ionosphere can become unstable to a Rayleigh-Taylor-like instability after sunset [*Sultan*, 1996]; this leads to large scale ($\lesssim$ 100 km) plasma bubbles that can rise to high altitudes ($\sim$ 1000 km) [*Ossakow*, 1981; *Kelley*, 1989; *Hysell*, 2000]. Associated with these bubbles, secondary fluid instabilities can develop on the 'walls' of the bubbles [*Haerendel*, 1974], as well as kinetic instabilities [*Huba et al.*, 1978]. This phenomenon is generally known as equatorial spread F (ESF) because it 'spreads' the return radio signal from ionosondes [*Booker and Wells*, 1938]. It is a concern because ESF causes the scintillation of radio signals that can degrade and disrupt communications and navigation systems.

Recently *Huang et al.* (2011) and *Huang et al.* (2012) reported observations of broad plasma depletions measured by the C/NOFS satellite during the last deep solar minimum. They suggest that these broad depletions form by the merging of multiple plasma bubbles and presented the results of a simulation study using PBMOD demonstrating the merging of two bubbles [*Retterer*, 2005; *Huang et al.*, 2012]. Similar behavior was observed in earlier simulations of equatorial spread F [*Huba and Joyce*, 2007].

In this paper we reexamine plasma bubble merging using the NRL code SAMI3/ESF. We find that bubbles merge through an 'electrostatic reconnection' process. As multiple bubbles develop, the electrostatic potential associated with one bubble can connect with that of a neighboring bubble which provides a pathway for the low density plasma in one bubble to flow into the adjoining bubble and merge with it. We also find that during the merging process high-speed plasma channels ($\gtrsim$ 100s m/s) can develop. We present optical data of equatorial plasma bubble evolution that suggests bubble merging occurs.

MODEL

The NRL 3D equatorial spread F code SAMI3/ESF [*Huba et al.*, 2008] is used in this study. It is initialized using results from the two-dimensional SAMI2 code [*Huba et al.*, 2000]. SAMI2 is run for 48 hrs using the following geophysical parameters: F10.7 = 120, F10.7A = 120, Ap = 4, geographic longitude 0°, and day-of-year 97 (e.g., 6 April 2012). The plasma parameters (density, temperature, and velocity) at time 1920 UT (of the second day) are used to initialize the 3D model at each magnetic longitudinal plane. SAMI3/ESF has recently been upgraded to use a 4th order, flux corrected transport scheme (the partial donor cell method) for $\mathbf{E} \times \mathbf{B}$ transport [*Hain*, 1987; *Huba*, 2003] and can now model the bifurcation and complex structuring of equatorial plasma bubbles.

We assume a magnetic dipole field aligned with the spin axis of the earth so geographic and geomagnetic coordinates are the same. The 3D model uses a grid with magnetic apex heights from 90 km to 2400 km, and a longitudinal width of 4° (e.g., $\simeq$ 460 km). The range of latitudes modeled is ±31° at the base of the field lines in each hemisphere. The grid is (nz, nf, nl) = (201,200,192) where nz is the number grid points along each magnetic field line, nf the number in 'altitude,' and nl the number in longitude. This grid has a resolution of $\sim$ 6 km × 2.5 km in altitude and longitude in the magnetic equatorial plane. The grid is periodic in longitude. In essence we are simulating a narrow 'wedge' of the ionosphere in the post-sunset period in the range -2° to +2°. A Gaussian-like perturbation in the ion density is imposed at $t = 0$. A 15% ion density perturbation is centered at 0°, ±0.8°, and ±1.6° longitude with a half-width of 0.35° so that the system is initialized to generate multiple bubbles. The perturbed ion density at the boundaries is enhanced by $\sim$ 1% so that an asymmetry is introduced at $t = 0$ at ±2°. The altitude of the perturbation is at z = 400 km with a half-width of 38.5 km. For simplicity and clarity, the neutral wind is set to zero.

MODELING RESULTS

In Fig. 1 we show color-coded contours of the electron density as a function of longitude and altitude at four times: 22:00 UT, 22:46 UT, 23:02 UT, and 23:14 UT. At time 22:00 UT the multi-bubble system has developed from the initial perturbation. We also note that the bubbles at ±1.6° have risen slightly higher than the interior bubbles because of the asymmetric initial perturbation. At time 22:46 UT, the bubbles have bifurcated and have risen to over 500 km. We highlight two bubbles: labeled A and B. At time 23:02 bubble B has moved closer to bubble A. Finally, at time 23:14 UT bubble B has merged with bubble A.

In order to understand the merging process we present Fig. 2. This is the same as Fig. 1 except we have limited the spatial range and show only three times at one minute intervals: 22:48 UT, 22:49 UT, and 22:50 UT. Additionally we show contours (white lines) of the electrostatic potential and highlight a single potential contour level shown in dark red. The potential contours are also indicative of the plasma $\mathbf{E} \times \mathbf{B}$ flow. In the top panel, at time 22:48 UT, the direction of plasma flow (arrows) is shown on each of the dark read potential contours. The flow is clockwise on the right side of both bubbles A and B. However, the flows are oppositely directed where the potential contours are closest. At time 22:49 UT the

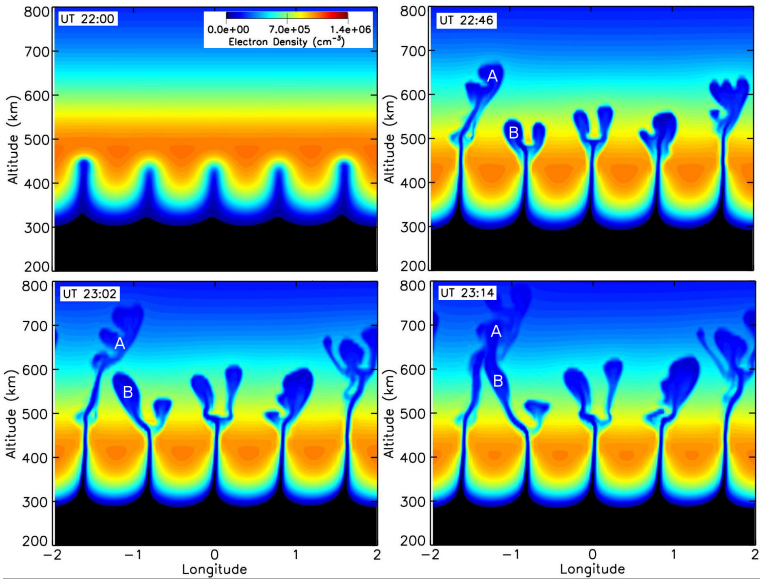

Figure 1: Color-coded contours of the electron density as a function of longitude and altitude at four times: 22:02 UT, 22:46 UT, 23:02 UT, and 23:14 UT.

potential contour lines have reconnected and bubble B is now directly coupled to bubble A. Finally, at time 22:50 UT the process continues and plasma in bubble B can begin to flow into bubble A. It is the direct connection of the electrostatic potential between bubbles A and B that allows bubble B to merge with bubble A as shown in the lower right panel of Fig. 1.

OBSERVATIONAL RESULTS

A wide-angle imaging system, the Portable Ionospheric Camera and Small Scale Observatory (PICASSO), was installed on Tahiti (geographic: 17.56 S, 210.43 E; geomagnetic: 15.03 S, 285.73 E) at the end of January 2014. By utilizing narrowband interference filters, PICASSO obtains images of specific nightglow emissions that naturally occur in the earths ionosphere/thermosphere over an approximately 120° field-of-view. Here, we use images of the emission occurring at 630.0 nm, caused by the dissociative recombination of O_2^+ [*Link and Cogger*, 1988], which has a peak emission altitude of approximately 250 km. This emission has a long history of being used to study the spatio-temporal development of equatorial plasma bubbles (EPBs), which show up in the images as elongated dark bands, typically moving from west to east (see *Makela* (2006) and references therein). The wide field-of-view of PICASSO, approximately 1000 km at the altitude of the 630.0-nm emission, allows the simultaneous observation of multiple EPBs as they drift over the observation site. The high temporal cadence of the images, approximately 2-3 minutes, allows for studying the development of the primary and secondary depletion structures.

In Fig. 3 we present four images of equatorial plasma bubbles from Tahiti using PICASSO

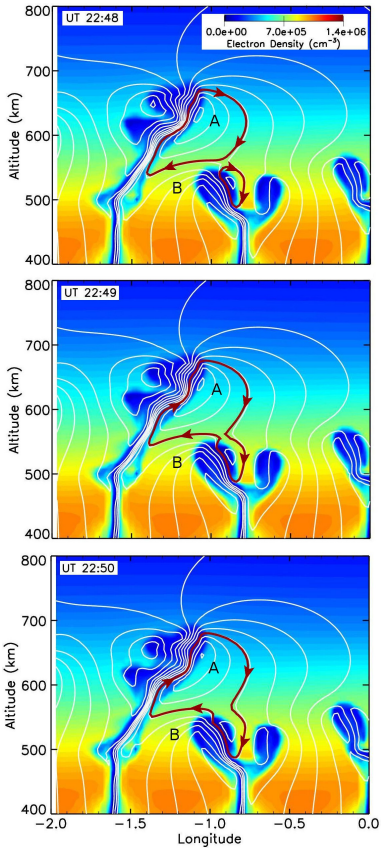

Figure 2: Color-coded contours of the electron density as a function of longitude and altitude at three times: 22:48 UT, 22:49 UT, and 22:50 UT. The electrostatic potential contours are shown in white, with a single contour value highlighted in dark red. The arrows on this contour level indicate the direction of plasma flow.

to image the 630.0-nm emission on July 5, 2014. The image times are 00:09:19 LT (a), 00:23:03 LT (b), 00:36:48 LT (c), and 00:50:32 LT (d) (roughly 14 min apart). Because the imaging system is in the southern hemisphere, the bubbles form at the top of each panel and rise toward the bottom of each panel (i.e., to larger latitudes). We label two bubbles A and B similar to the labeling in Fig. 1. In panel (a) the two bubbles are distinct and separated. In panel (b) bubble B has bifurcated and is moving towards bubble A. In panel (c) bubble B appears to be merging with bubble A. And lastly, in panel (d) the two bubble B has merged with bubble A. This sequence is very similar to the simulation results shown in Fig. 1.

SUMMARY

We have studied the merging of equatorial plasma bubbles using the NRL code SAMI3/ESF. It appears that bubbles merge through an 'electrostatic reconnection' process: as multiple bubbles develop, the electrostatic potential associated with one bubble can connect with that of a neighboring bubble which allows a pathway for the low density plasma in one

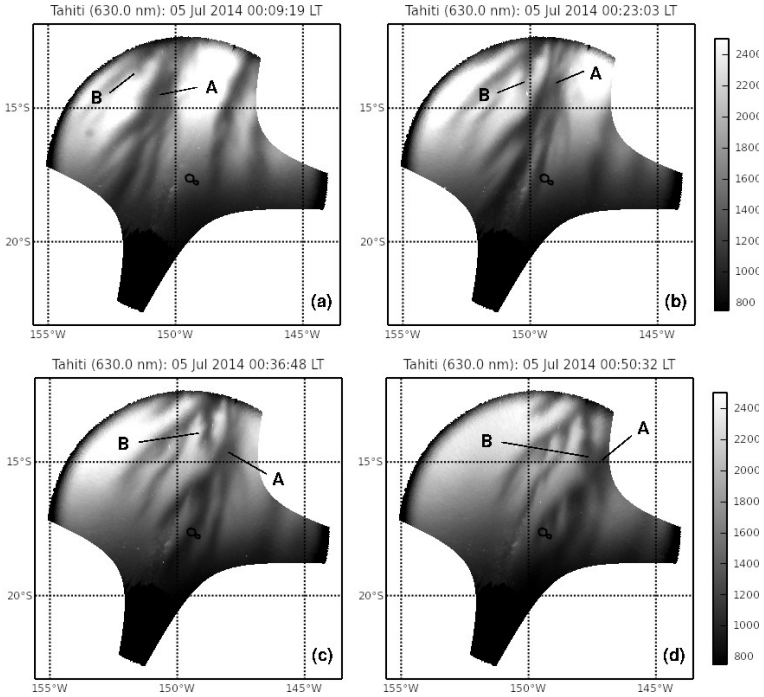

Figure 3: Four images of equatorial plasma bubbles from Tahiti using PICASSO on July 5, 2014.

bubble to flow into the adjoining bubble. For this to occur there must be a diffusive process (e.g., collisionality) that allows reconnection to occur and a change in topology (i.e., flow fields). This is analogous to the physics of magnetic reconnection. Additionally, for this to occur there must be a strong asymmetry in adjacent bubbles such that the $\mathbf{E} \times \mathbf{B}$ flows are oppositely directed, i.e., the vorticity ($\nabla \times \mathbf{V}$) is the same sign between the two merging bubbles. We have also presented optical data of equatorial plasma bubble evolution that suggests bubble merging occurs. However, this merging process does not appear to lead to significantly broader depletions. Further details can be found in *Huba et al.* (2015).

ACKNOWLEDGMENTS

One of us (JDH) thanks Dave Hysell for helpful discussions. The research of JDH and TWW has been supported by an LWS NASA grant and NRL Base Funds. Work at the University of Illinois was support by the Office of Naval Research through grant N00014-13-1-0350. We thank Dominique Reymond and colleagues at the Laboratories de Geophysique in Tahiti for supporting the deployment of the PICASSO imaging system. Modeling data is available from JDH and optical data from JJM.

REFERENCES

Booker, H.G. and H.G. Wells, Scattering of radio waves by the F-region of the ionosphere, *Terr. Mag. Atmos. Elec. 43*, 249, 1938.

Haerendel, G., Theory of equatorial spread F, preprint, Max-Planck Inst. für Extraterr. Phys., Munich, Germany, 1974.

Hain, K., The partial donor cell method, *J. Comput. Phys. 73*, 131, 1987.

Huang, C.-S., O. de La Beaujadiere, P.A. Roddy, D.E. Hunton, R.F. Pfaff, C.E. Valladares, and J.O. Ballenthin, Evolution of equatorial ionospheric plasma bubbles and formation of broad plasma depletions measured by the C/NOFS satellite during deep solar minimum, *J. Geophys. Res. 116*, A03309, doi:10.1029/2010JA015982, 2011.

Huang, C.-S., J.M. Retterer, O. de La Beaujadiere, P.A. Roddy, D.E. Hunton, J.O. Ballenthin and R.F. Pfaff, Observations and simulations of formation of broad plasma depletions through merging process, *J. Geophys. Res. 117*, A02314, doi:10.1029/2011JA017084, 2012.

Huba, J.D., P.K. Chaturvedi, S.L. Ossakow and D.M. Towle, High frequency drift waves and wavelengths below the ion gyroradius in equatorial spread F, *Geophys. Res. Lett. 5*, 695, 1978.

Huba, J. D., G. Joyce, and J. A. Fedder (2000), SAMI2 (Sami2 is Another Model of the Ionosphere): A New Low-Latitude Ionosphere Model, *J. Geophys. Res.*, *105*, 23,035.

Huba, J.D., A tutorial on Hall magnetohydrodynamics, in *Space Simulations*, eds. M. Scholer, C.T. Dum, and J. Büchner (Springer, New York) p. 170, 2003.

Huba, J. D. and G. Joyce, Equatorial spread F modeling: Multiple bifurcated structures, secondary instabilities, large density 'bite-outs' and supersonic flows, *Geophys. Res. Lett. 34*, L07015, doi:10.1029/2006GL028519, 2007.

Huba, J.D., G. Joyce and J. Krall, Three-dimensional equatorial spread F modeling, *Geophys. Res. Lett. 35*, L10102, doi:10.1029/2008GL033509, 2008.

Huba, J.D., T.-W. Wu, and J.J. Makela, Electrostatic reconnection in the ionosphere, *Geophys. Res. Lett. 42*, doi:10.1002/2015GL063187, 2015.

Hysell, D.L., An overview and synthesis of plasma irregularities in equatorial spread F, *J. Atmos. Sol. Terr. Phys. 62*, 1037, 2000.

Kelley, M.C., *The Earth's Ionosphere*, Academic Press, San Diego, CA, 1989.

Kelley, M.C., J.J. Makela, B.M. Ledvina, and P.M. Kintner, Observations of equatorial spread-F from Haleakala, Hawaii, *Geophys. Res. Lett. 29*, 2003, doi:10.1029/2002GL015509, 2002.

Link, R. and L.L. Cogger, A reexamination of the OI 6300-Å nightglow, *J. Geophys. Res. 93*, 9883, 1988.

Makela, J.J., A review of imaging low-latitude ionospheric irregularity processes, *J. Atomos. Solar-Terr. Phys. 68*, 1441, 2006.

Ossakow, S.L., Spread F theories: A review, *J. Atmos. Terr. Phys., 43*, 437, 1981.

Retterer, J.M., Physics-based forecasts of equatorial radio scintillation for the Communication and Navigation Outage Forecasting System, (C/NOFS), *Space Weather 3*, S12C03, doi:10.1029/2005SW000146, 2005.

Sultan, P.J., Linear theory and modeling of the Rayleigh-Taylor instability leading to the occurrence of equatorial spread F, *J. Geophys. Res. 101*, 26,875, 1996.